2015 IEEE International Conference on Advanced Intelligent Mechatronics (AIM)
July 7-11, 2015. Busan, Korea

Dexterity and Functionality Enhancement of the SJTU Unfoldable Robotic System

Kai Xu*, *Member, IEEE*, Zhengchen Dai, *Student Member, IEEE*,
Jiangran Zhao, *Student Member,* and Wukun Mei

***Abstract*—SPL (Single Port Laparoscopy) received more and more attention due to the potential of generating better surgical outcomes than multi-port laparoscopy. Several robotic systems were constructed to allow surgeons to operate in an intuitive way so as to ease the challenges of using manual SPL tools. The SURS (SJTU Unfoldable Robotic System) is one of the recent developments dedicated for SPL. The SURS can be inserted into abdomen through a Ø12mm incision in its folded configuration and can then be unfolded for dual-arm interventions with integrated visual guidance. With the design descriptions, modeling and experimentation reported in a recent manuscript, this paper presents the follow-up investigations to enhance the SURS's capabilities. Bending ranges of the continuum manipulation arms are enlarged to enhance the system's distal dexterity. An additional tool with an electrical cautery spatula was fabricated and assembled into the system to realize tissue resection. With the dexterity and functionality augmented, the SURS could be further tested in animal studies.**

I. Introduction

SPL (Single Port Laparoscopy) often uses umbilicus for surgical interventions [1]. Compared with traditional multi-port laparoscopy, SPL could generate better surgical outcomes [2]. Although emerging manual tools have enabled SPL procedures, the tool manipulation is still very difficult due to the crossed and inversed hand-eye coordination. Surgeons might need to receive substantial training to master these new tools, such as the RealHand^{TM} tools and the Laparo-Angle^{TM} instruments.

Several robotic systems were built, aiming at allowing surgeons to operate intuitively in SPL procedures. Sekiguchi *et al.* developed the SPS (Single Port Surgery) robot with two 5-DoF arms using a Ø30mm incision [3]. An updated version has two 6-DoF arms and uses a Ø25mm incision [4]. The SPL robots developed by Lee *et al.* and Cheon *et al.* both use Ø25mm incisions [5, 6]. Titan Medical Inc. announced its SPORT^{TM} (Single Port Orifice Robotic Technology) Surgical System with two 8-DoF arms and 3.25N payloads using a Ø25mm incision [7]. The da Vinci SP system was also released recently which has three 7-Dof arms and uses a Ø25mm access port [8]. Picciagallo *et al.* constructed the SPRINT (Single-Port lapaRoscopy bImaNual roboT) robot for SPL with two 6-DoF arms, using a Ø23mm incision [9]. A modified version is reported in [10] with two 6-DoF arms using a Ø30mm access port. Ding *et al.* developed the IREP (Insertable Robotic Effectors Platform) robot for SPL [11, 12]. It has two 7-DoF manipulation arms and can be deployed through a Ø15mm port. When other specifications (e.g., dexterity, payload, workspace, etc.) are comparable, a key specification of these SPL robots could be considered the diameter of the access port. A smaller access port might lead to even less invasiveness but could substantially complicate the design of such a surgical robot.

Aiming to push the design boundary of SPL robots, the SURS (SJTU Unfoldable Robotic System) for SPL was recently developed as shown in Fig. 1. Its design was reported in [13] with comprehensive experimental characterizations detailed in [14], including the system deployment, actuation compensation, stiffness characterization, and teleoperation for knot tying, grape skin peeling, etc. The SURS can be deployed into abdomen through a Ø12mm skin incision in the folded configuration and can then be unfolded to form a dual-arm working configuration. It consists of two 6-DoF manipulation arms and one 3-DoF vision unit.

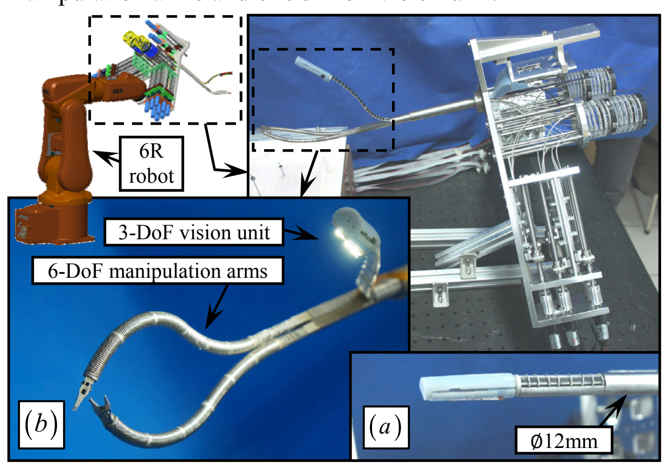

Fig. 1.The SURS robot: (a) the folded configuration with an outer diameter of 12mm, and (b) the unfolded working configuration

During the ex-vivo experimentation of the SURS, it was found that the workspace and the distal dexterity shall be enhanced. Many desired motions cannot be accomplished in one move in the tasks of knot tying, ring placing, grape skin peeling, etc. due to the limited workspace and/or the limited directions in which the gripper could be oriented. These tasks had to be completed incrementally. Many intermediate steps,

Manuscript received Feb 20*th*, 2015. This work is supported in part by the GRO (Global Research Outreach) program of the SAIT (Samsung Advanced Institute of Technology), in part by the National Natural Science Foundation of China (Grant No. 51375295), and in part by the Shanghai Rising-Star Program (Grant No. 14QA1402100).

The authors are with the RII Lab (Lab of Robotics Innovation and Intervention), UM-SJTU Joint Institute, Shanghai Jiao Tong University, Shanghai, 200240, China (asterisk indicates the corresponding author, phone: 86-21-34207220; fax: 86-21-34206525; emails: [k.xu, zhengchendai, zjr318 and meiwk1005]@sjtu.edu.cn).

978-1-4673-9107-8/15/$31.00 ©2015 IEEE

such as passing and handing over, had to be included. It may be perceived that the manipulation arms are not dexterous enough.

The continuum manipulation arms were not dexterous enough because the bending shape of each segment was only characterized and hence limited to a 90° bending as in [14]. Their bending capabilities should be fully utilized via proper kinematic modeling and experimental characterization.

This paper proposes the kinematics model to be used for extended bending configurations, fully describing the motion capabilities of the SURS's manipulation arms. The motion capabilities are also experimentally verified. What's more, both arms are with grippers in the previous study. A third arm with an electrical cautery spatula was fabricated and assembled into the system to realize tissue resection.

Main contributions of this paper hence include i) extension of the kinematics modeling for a bending beyond 90° with experimental verifications, ii) quantification of the improved dexterity of the manipulation arms, and iii) integration of an electrical cautery spatula for functionality enhancement.

This paper is organized as follows. Section II briefly summarizes the design objectives and the component descriptions of the SURS, including the new arm with an electrical cautery spatula. Section III presents the nomenclature and an extended kinematics to quantify the enhanced motion capabilities of the manipulation arms. Experimental verification of the motion capabilities and demonstration of the tissue resection are reported in Section IV, with conclusions summarized in Section V.

II. Design Overview and Descriptions

The SURS was constructed as in Fig. 1. It could be carried and positioned by a standard 6R industrial robot. The robot acts as a RCM (Remote Center of Motion) mechanism and pivots the stem of the SURS around the incision point in the abdomen wall.

The SURS consists of two main components: i) the vision unit with integrated illumination, and ii) the manipulation arms with actuation. A control system was also implemented to allow teleoperation of the SURS. With details presented in [13, 14], this section briefly summarizes the component descriptions.

A. The Vision Unit

In order to facilitate its insertion through a skin incision, the vision unit can be folded into a cylindrical form as in Fig. 1(a). After insertion, the vision unit could be extended and bent upwards to provide visualization and illumination of the surgical site, as shown in Fig. 2. The vision unit consists of a camera head and a 2-segment continuum camera arm.

The Ø12mm camera head possesses two MO-BL1204LK camera chips (Misumi Inc.) with a resolution of 640×480. The two chips were placed side by side for stereo vision.

Ten LEDs are mounted on the surface. They have a nominal voltage of 2.95v but are powered at 2.70v to avoid the heating problem but supply enough illumination.

The 2-segment continuum arm orients and positions the camera head. It mainly consists of a nitinol strip, several spacer rings, and two nitinol rods. The rods are attached to the distal end and the middle point of the nitinol strip. Pushing and pulling the rods deflect the strip into two bending segments. The distal segment is 60mm long and the proximal one is 40mm long to realize a viewing range from 120mm to 170mm. Besides bending of the two segments, the arm can also be fed from the stem. The camera arm is hence driven by three motorized ball screws as in Fig. 2.

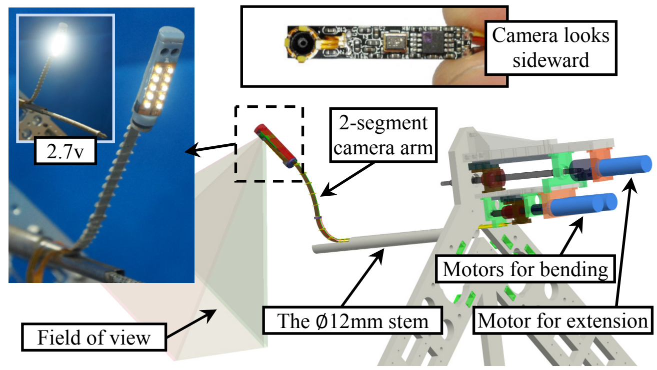

Fig. 2.The vision unit with integrated illumination

B. Continuum Manipulation Arms with Actuation

The SURS's capabilities largely depend on those of its manipulation arms. The topological structure of the SURS's arms was carefully selected in order to not only achieve satisfactory kinematic performance but also ensure the design compactness. According to the comparison of the kinematic performances of three continuum manipulators [15, 16], a 2-segment 6-DoF structure was used as shown in Fig. 3.

The manipulation arm in Fig. 3(a) consists of a gripper, the DS-2 (Distal Segment #2), the DS-1 (Distal Segment #1), the PS-1 (Proximal Segment #1), the PS-2 (Proximal Segment #2), and the bounded cannulae.

The DS-1 is similar to the DS-2. Each segment consists of three serially connected FC-4 nickel bellows (Servometer LLC.). The bellows all are 6.35mm in diameter and 18.8mm long. They can be easily bent, compressed and stretched. Eighteen Ø0.5mm holes were drilled in the bellows' convolutions by wire EDM as in the inset of Fig. 3(a).

Nine Ø0.40mm nitinol rods as the DS-1's backbones are attached to the DS-1's distal end. The backbones are routed through the DS-1, the cannulae, the PS-1, and attached to the proximal end of the PS-1. Nine more Ø0.40mm nitinol rods as the DS-2's backbones are attached to the DS-2's distal end, routed through the DS-2, the DS-1, the cannulae, the PS-1, and the PS-2, and attached to the proximal end of the PS-2.

The DS-1 and the DS-2 both have 3 DoFs: a 2-DoF bending and a 1-DoF compression/extension. The PS-1's bending would bend the DS-1 in the opposite direction; extending the PS-1 would shorten the DS-1 and vice versa. Actuation of the PS-2 would drive the DS-2 similarly. This actuation duality results from the fact that the arrangement of the backbones in the DS-1 and the DS-2 is similar and scaled to that in the PS-1 and the PS-2.

The manipulation arm can be inserted into the SURS for actuation. The insertion is in place when the fixtures (BRF-1 and BRF-2) of the arm as in Fig. 3(a) match the fixtures (BRF-1 and BRF-2) in the SURS as in Fig. 3(b). Retaining pins can be inserted to lock the arms. The SURS's fixture BRF-2 in Fig. 3(b) has a C shape to allow the arm to pass. Then a telescoping rod in Fig. 3(b) would be connected to the slider in Fig. 3(a) to drives the gripper.

The cross section of the SURS' stem is shown in the left side of Fig. 3(c) when one arm is fully inserted and the other is being inserted. The backbones in the cannulae are bounded so to allow two Ø6.35mm arms to be inserted through a Ø12mm stem one by one.

Eight backbones shown in Fig. 3(b) would be connected to the proximal ends of the PS-1 and the PS-2. They would be pushed and/or pulled to bend and/or extend/shorten the PS-1 and the PS-2 so as to drive the DS-1 and the DS-2. The gripper and these backbones are all driven by ball screws.

The gripper can be replaced by an electrical cautery spatula as shown in Fig. 3(a). A third arm with such a spatula was recently fabricated to realize tissue resection. The spatula is connected to a generator (DGD-300C-2, Beilin Electronics Inc). The cutting can be initiated by stepping on a pedal.

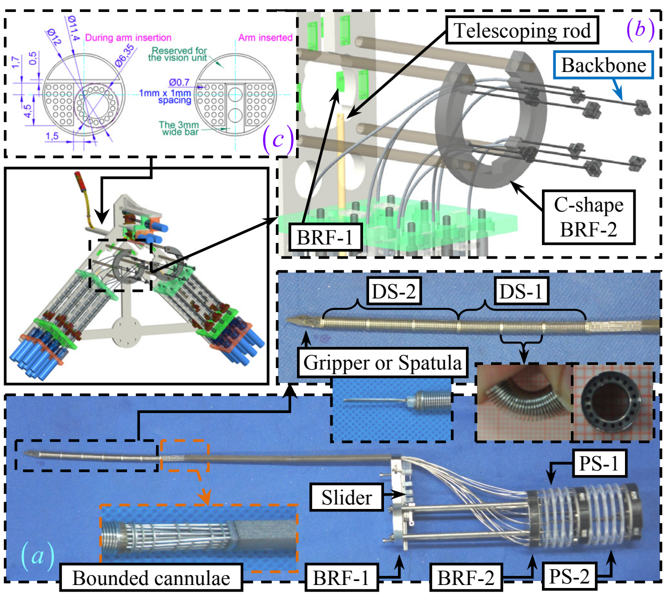

Fig. 3.Manipulation arms and its actuation assembly

C. Control Infrastructure

The SURS's control infrastructure adopts a conventional setup for teleoperation.

As shown in Fig. 4, two Phantom Omni devices (Sensable Inc.) were connected to a Host PC via IEEE 1394 firewires to provide control inputs. The Host PC runs a Windows-based program that sends the tip positions and orientations from the two Omni devices to two Target PCs via a router with LAN connections using a UDP (User Datagram Protocol) every 10 milliseconds.

Each Target PC controls one manipulation arm under a real-time OS generated by MATLAB's xPC module. The duration of the servo loop is 1 millisecond.

Multiple motion control cards, including the PCL727 D/A cards (AdvanTech Inc.) and the CNT32-8M counter cards (ConTec Inc.), are used. The motors (A-max series) and the amplifiers (LSC 30/2) are from Maxon Inc.

During each servo loop, the controller generates control signals according to the inputs from the Omni devices and the inverse kinematics of the arm. During the teleoperation, the 3-DoF vision unit is currently kept stationary.

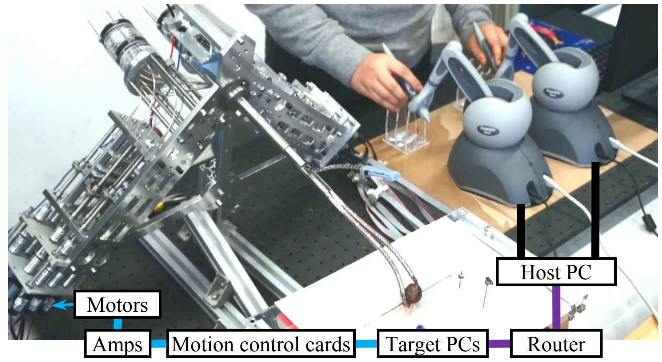

Fig. 4.The SURS's control infrastructure for teleoperation

III. Kinematics and Distal Dexterity Enhancement

The manipulation arms were designed so according to the kinematic performance comparison in [15, 16]. In that study, the arm's distal dexterity is better than other candidates when each segment can bend for 90° and extend/contract ±40% of its original length. In the actual implementation, a segment's extension/contraction is limited by the bellows used in the structure. When the segments are still only allowed for a 90° bending, the distal dexterity is below the expectation. However, each segment can bend more. The 90° bending is only limited by the range of a configuration variable.

In this paper, the kinematics is derived and verified for a bending beyond 90°. The improvement of the distal dexterity is then quantified.

The arm consists of several similar continuum segments: the DS-1, the DS-2, the PS-1 and the PS-2. The *t*th segment (*t*=1 or 2) is shown in Fig. 5(a). Then the arm's kinematics is obtained using the kinematics of the *t*th segment. Kinematics of the PS-1 and PS-2 could be obtained similarly if needed.

A. Nomenclature and Coordinate Systems

The nomenclatures are defined in Table I, while four coordinate systems of the *t*th segment are defined as below:

- *Base Ring Coordinate* $\{tb\} \equiv \{\hat{\mathbf{x}}_{tb}, \hat{\mathbf{y}}_{tb}, \hat{\mathbf{z}}_{tb}\}$ has its XY plane aligned with the base ring of the *t*th segment. The origin is at the ring center. $\hat{\mathbf{x}}_{tb}$ points from the center to the first backbone while $\hat{\mathbf{z}}_{tb}$ is perpendicular to the ring.
- *Bending Plane Coordinate 1* $\{t1\} \equiv \{\hat{\mathbf{x}}_{t1}, \hat{\mathbf{y}}_{t1}, \hat{\mathbf{z}}_{t1}\}$ shares its origin with $\{tb\}$ and has the continuum segment bending in its XZ plane.
- *Bending Plane Coordinate 2* $\{t2\} \equiv \{\hat{\mathbf{x}}_{t2}, \hat{\mathbf{y}}_{t2}, \hat{\mathbf{z}}_{t2}\}$ is obtained from $\{t1\}$ by a rotation about $\hat{\mathbf{y}}_{t1}$ such that

$\hat{\mathbf{z}}_{t1}$ becomes backbone tangent at the end ring. Origin of $\{t2\}$ is at center of the end ring.

- *End Ring Coordinate* $\{te\} \equiv \{\hat{\mathbf{x}}_{te}, \hat{\mathbf{y}}_{te}, \hat{\mathbf{z}}_{te}\}$ is fixed to the end ring of the *t*th segment. $\hat{\mathbf{x}}_{te}$ points from the ring's center to the first backbone and $\hat{\mathbf{z}}_{te}$ is normal to the ring. $\{te\}$ is obtained from $\{t2\}$ by a rotation about $\hat{\mathbf{z}}_{t2}$.

When the *2*nd segment is stacked on top of the *1*st segment, $\{1e\}$ coincides with $\{2b\}$.

TABLE I
NOMENCLATURE USED IN KINEMATICS MODELING

Symbol	Representation
i	Index of the backbones, $i = 1, 2, \ldots, m$
t	Index of the segments $t = 1, 2$; t always precedes i.
r_{ti}	Distance from the virtual central backbone to the *i*th backbone in the *t*th segment.
β_{ti}	β_{ti} characterizes the division angle from the *i*th backbone to the *1*st backbone in the *t*th segment. $\beta_{t1} \equiv 0$ and β_{ti} remain constant once the manipulation arm is built.
L_t, L_{ti}	Length of the central and the *i*th backbone for the *t*th segment.
$\theta_t(s)$	The angle of the tangent to the central backbone in the bending plane for the *t*th segment. $\theta_t(L_t)$ and $\theta_t(0)$ are designated by θ_{tL} and θ_0. $\theta_0 = \pi/2$ is a constant.
$\bar{\theta}_{tL}$	$\bar{\theta}_{tL} \equiv \pi/2 - \theta_{tL}$. Due the definition of θ_{tL}, $\theta_{tL} = 0$ represents a 90° bending. $\bar{\theta}_{tL}$ provides an intuitive indication of bending.
δ_{ti}	A right-handed rotation angle from $\hat{\mathbf{x}}_{t1}$ about $\hat{\mathbf{z}}_{t1}$ to a ray passing through the central and the *i*th backbones.
δ_t	$\delta_t \equiv \delta_{t1}$ and $\delta_{ti} = \delta_t + \beta_{ti}$
$\boldsymbol{\psi}_t$	$\boldsymbol{\psi}_t = [\theta_{tL} \ \ \delta_t \ \ L_t]^T$ is a configuration vector which defines the pose of the *t*th segment.
${}^{1}\mathbf{R}_2$	Coordinate transformation matrix from frame *2* to frame *1*.
${}^{tb}\mathbf{p}_t(s)$	Position vector of a point along the primary backbone in $\{tb\}$. ${}^{tb}\mathbf{p}_t(L_t)$ is the tip position designated by ${}^{tb}\mathbf{p}_{tL}$.

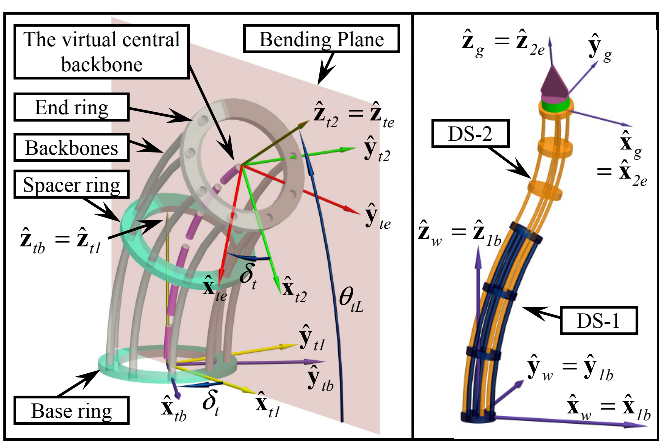

Fig. 5.Nomenclature and coordinates of (a) the *t*th segment and (b) the arm

B. Kinematics of the *t*th Segment

The virtual central backbone characterizes the length and the shape of one segment. The kinematics assumes a circular shape for the segments. This assumption was widely adopted [17-19] and experimentally verified with bending up to 90° [18, 20]. The experiments in Section IV.A verify this assumption for the bending beyond 90°.

The kinematics was presented in detail in [14]. It is briefly summarized here for completeness.

Shape of the *t*th continuum segment can be characterized by $\boldsymbol{\psi}_t$ as in Table I. Then the tip position is as follows:

$$ {}^{tb}\mathbf{p}_{tL} = \frac{L_t}{\theta_{tL} - \theta_0} \begin{bmatrix} \cos\delta_t (\sin\theta_{tL} - 1) \\ \sin\delta_t (1 - \sin\theta_{tL}) \\ -\cos\theta_{tL} \end{bmatrix} \tag{1} $$

Where ${}^{tb}\mathbf{p}_{tL} = [0 \ \ 0 \ \ L_t]^T$ when $\theta_{tL} = \theta_0 = \pi/2$.

Coordinate transformation matrix ${}^{tb}\mathbf{R}_{te}$ is written as:

$$ {}^{tb}\mathbf{R}_{te} = \mathrm{R}(\hat{\mathbf{z}}_{tb}, -\delta_t)\mathrm{R}(\hat{\mathbf{y}}_{t1}, \theta_0 - \theta_{tL})\mathrm{R}(\hat{\mathbf{z}}_{t2}, \delta_t) \tag{2} $$

Where $\mathrm{R}(\hat{\mathbf{n}}, \gamma)$ defines a rotation about $\hat{\mathbf{n}}$ by an angle γ.

The instantaneous kinematics is then given by:

$$ \dot{\mathbf{x}}_t = \mathbf{J}_{tx\psi}\dot{\boldsymbol{\psi}}_t \ \text{ where } \mathbf{J}_{tx\psi} = \begin{bmatrix} \mathbf{J}_{tv} \\ \mathbf{J}_{t\omega} \end{bmatrix} \tag{3} $$

$$ \mathbf{J}_{tv} = \begin{bmatrix} L_t c_{\delta_t} \frac{(\theta_{tL} - \theta_0)c_{\theta_{tL}} - s_{\theta_{tL}} + 1}{(\theta_{tL} - \theta_0)^2} & -L_t \frac{s_{\delta_t}(s_{\theta_{tL}} - 1)}{\theta_{tL} - \theta_0} & \frac{c_{\delta_t}(s_{\theta_{tL}} - 1)}{\theta_{tL} - \theta_0} \\ -L_t s_{\delta_t} \frac{(\theta_{tL} - \theta_0)c_{\theta_{tL}} - s_{\theta_{tL}} + 1}{(\theta_{tL} - \theta_0)^2} & -L_t \frac{c_{\delta_t}(s_{\theta_{tL}} - 1)}{\theta_{tL} - \theta_0} & \frac{s_{\delta_t}(1 - s_{\theta_{tL}})}{\theta_{tL} - \theta_0} \\ L_t \frac{(\theta_{tL} - \theta_0)s_{\theta_{tL}} + c_{\theta_{tL}}}{(\theta_{tL} - \theta_0)^2} & 0 & \frac{-c_{\theta_{tL}}}{\theta_{tL} - \theta_0} \end{bmatrix} \tag{4} $$

$$ \mathbf{J}_{t\omega} = \begin{bmatrix} -s_{\delta_t} & c_{\delta_t} c_{\theta_{tL}} & 0 \\ -c_{\delta_t} & -s_{\delta_t} c_{\theta_{tL}} & 0 \\ 0 & -1 + s_{\theta_{tL}} & 0 \end{bmatrix} $$

C. Kinematics and Dexterity of the Manipulation Arm

The DS-2 is serially connected the DS-1 to form the arm. The coordinates are assigned as in Fig. 5(b). A configuration vector $\boldsymbol{\xi} = \begin{bmatrix} \boldsymbol{\psi}_2^T & \boldsymbol{\psi}_1^T \end{bmatrix}^T$ parameterizes the arm. Kinematics of the *t*th segment is used to assemble the kinematics of the arm.

Tip position of the gripper in $\{w\}$ and the instantaneous kinematics can be derived as follows:

$$ {}^{w}\mathbf{p}_g = {}^{1b}\mathbf{p}_{1L} + {}^{1b}\mathbf{R}_{2b}\left({}^{2b}\mathbf{p}_{2L} + {}^{2b}\mathbf{R}_{2e}\,{}^{2e}\mathbf{R}_g\,{}^{g}\mathbf{p}_g\right) \tag{5} $$

Where ${}^{1b}\mathbf{p}_{1L}$ and ${}^{2b}\mathbf{p}_{2L}$ can be obtained from Eq. (1); and ${}^{g}\mathbf{p}_g$ is the gripper tip position in $\{g\}$.

$$ \dot{\mathbf{x}} = \mathbf{J}_{x\xi}\dot{\boldsymbol{\xi}} \tag{6} $$

$$ \mathbf{J}_{x\xi} = \begin{bmatrix} {}^{1b}\mathbf{R}_{2b}\left(\mathbf{J}_{2v} - \left[{}^{2b}\mathbf{R}_g\,{}^{g}\mathbf{p}_g\right]^{\times}\mathbf{J}_{2\omega}\right) & \mathbf{T}_{C1} \\ {}^{1b}\mathbf{R}_{2b}\mathbf{J}_{2\omega} & \mathbf{J}_{1\omega} \end{bmatrix} \tag{7} $$

Where $\mathbf{T}_{C1} = \mathbf{J}_{1v} - \left[{}^{1b}\mathbf{R}_{2b}\,{}^{2b}\mathbf{p}_{2L} + {}^{1b}\mathbf{R}_g\,{}^{g}\mathbf{p}_g\right]^{\times}\mathbf{J}_{1\omega}$, $[\mathbf{p}]^{\times}$ is the skew-symmetric matrix of a vector $\mathbf{p}$. Expressions of $\mathbf{J}_{1v}$, $\mathbf{J}_{1\omega}$, $\mathbf{J}_{2v}$ and $\mathbf{J}_{2\omega}$ are from Eq. (4).

According to the previous study in [14], the ranges of the configuration variables are summarized in the upper portion of Table II. The ranges for bending (θ_{tL}) are artificially limited to 90° and referred as to the AL case.

In the AL case, the translational workspace of one arm can be plotted as in Fig. 6(a) by scanning the configuration space. The workspace can barely envelop a functional volume of 50mm×50mm×40mm. The reason lies on the limited range of L_t due to the bellows' rated extension/contraction ranges.

Although the segment has a limited range for its extension or compression, it can bend more than 90°. This paper hence proposes to extend the configuration variables ranges for the enhanced bending, which is referred as to the EB case.

The variables ranges in the EB case are summarized in the lower portion of Table II. The bending ranges of the DS-1 and DS-2 are extended to 150° ($\underline{\theta}_{tL} = -\pi/3$, $\overline{\theta}_{tL} = 5\pi/6 = 150°$). Although each segment can bend 180° in the experiments in Section IV.A, the gripper can hit the base if both segments bend 180° at the same time.

The bellows will have one side extended and the other contracted when they are bent. Their bending will be limited, if they were already extended or contracted. This corresponds to the bending ranges when $L_t \le 50.6mm$ or $L_t \ge 59.4mm$.

The translational workspace of one arm can then be plotted as in Fig. 6(b) for the EB case, with the same functional volume. The improvement is obvious.

TABLE II
CONFIGURATION VARIABLES OF THE MANIPULATION ARMS

The AL case	$r_{ti} = 2.5mm$	$\delta_t \in [-\pi, \pi]$	$L_t \in [48mm, 62mm]$
$\theta_{tL} \in [0, \pi/2]$		${}^g\mathbf{p}_g = [0\ \ 0\ \ 15mm]^T$	
The EB case	$r_{ti} = 2.5mm$	$\delta_t \in [-\pi, \pi]$	$L_t \in [48mm, 62mm]$
$\begin{cases} \theta_{tL} \in [-(L_t - 48)/r_{ti}, \pi/2] \\ \quad \text{when } L_t \in [48mm, 50.6mm] \\ \theta_{tL} \in [-\pi/3, \pi/2] \\ \quad \text{when } L_t \in [50.6mm, 59.4mm] \\ \theta_{tL} \in [-(62 - L_t)/r_{ti}, \pi/2] \\ \quad \text{when } L_t \in [59.4mm, 62mm] \end{cases}$		${}^g\mathbf{p}_g = [0\ \ 0\ \ 15mm]^T$	

The increase in the workspace is only one aspect of the enhancement. In surgical applications, a surgeon also cares whether he or she can orient a surgical end effector freely, which concerns the dexterous workspace.

The translational workspace is not generally related to the dexterous workspace. But for the continuum arms with the bending segments, points on the translational workspace boundaries usually involve its segments in the straight or the maximally bent configurations. Zero or maximal bending reduces the dexterous workspace because the dexterous workspace depends on the segments' bending. With a bigger translational workspace, a surgeon can operate at points further away from the boundaries. The results below could echo this claim. More similar results could be found in [16].

The solid angle which could be swept by the gripper's axis is used to quantify the distal dexterity at one point as in [16]. Two representative points are selected: the volume center P_1 and the bottom surface center P_2 of the functional volume as in Fig. 7. The functional volume is placed at the same position for the two cases. The evaluated solid angle at the P_1 point is 2.47 sr (steradian) for the AL case and 3.03 sr for the EB case. The solid angle at the P_2 point is 0.19 sr for the AL case and 3.77 for the EB case. It can be clearly seen from Fig. 6 that the P_2 point is much closer to the workspace boundary in the AL case. The distal dexterity is hence much lower than the EB case.

Although a more thorough evaluation of the distal dexterity at various points could be carried out, the representative results at the two points well indicate the level of the distal dexterity improvement.

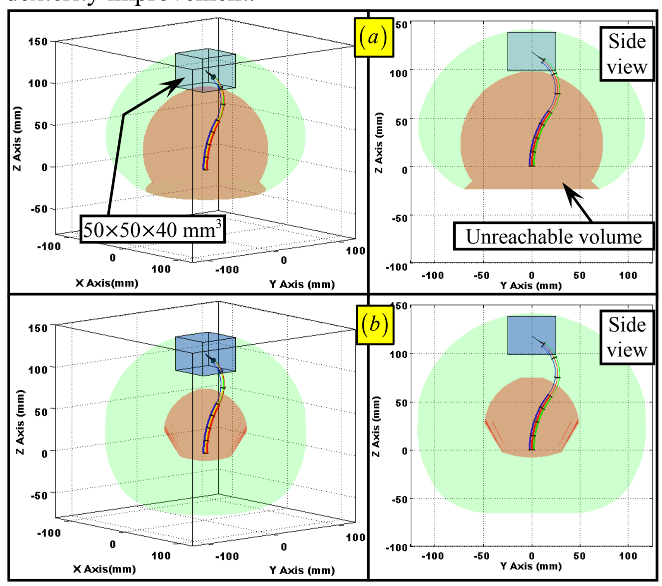

Fig. 6.Workspace of one arm: (a) the AL case and (b) the EB case

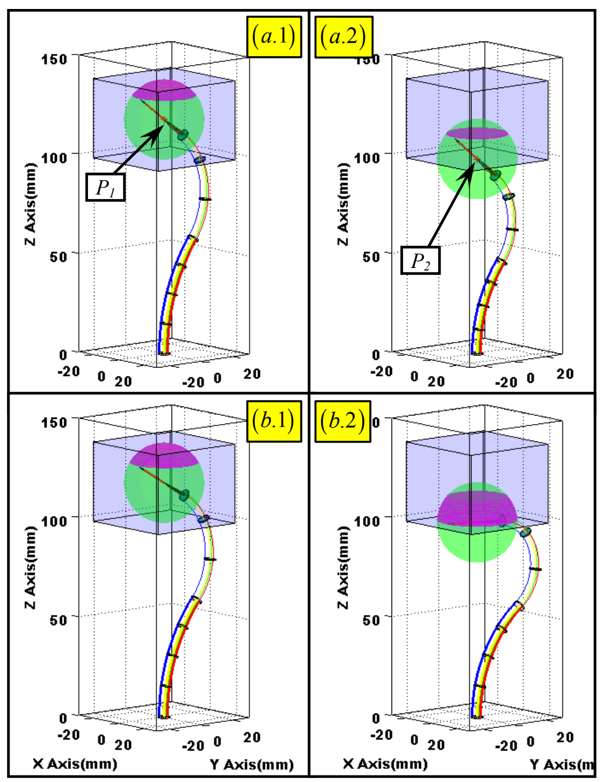

Fig. 7.Evaluation of the distal dexterity: (a) the AL case and (b) the EB case.

IV. Experimental Characterization

Various experiments have been carried out on the SURS, such as the system deployment, actuation compensation, stiffness characterization, teleoperation, etc. as in [14].

This paper proposes i) dexterity enhancement based on the segments' bending beyond 90°, and ii) functionality enhancement based on a new arm for electrical cautery. The presented experiments try to verify these enhancements.

A. Bending Characterization

The shape identification experiments were carried out to verify the assumption that the segments still bend into circular arcs even for bending beyond 90°.

The experiment is based on an imaging processing technique. Various pictures were taken for a segment that was bent to different angles. Edge detection was applied after the surrounding pixels were manually erased. All the points on the detected edges were used for curve fitting. Curve fitting results were overlaid back to the original picture to examine whether the fitted curves matched the shapes of the segments, as shown in Fig. 8.

Using the curve fitting results, bending angles ($\bar{\theta}_{tL}$) versus segment lengths can be plotted for the DS-1 and DS-2 as shown in Fig. 8. Similar techniques have been used in [20, 21]. It can be clearly seen from Fig. 8 that these bending shapes can still be well approximated by circular arcs.

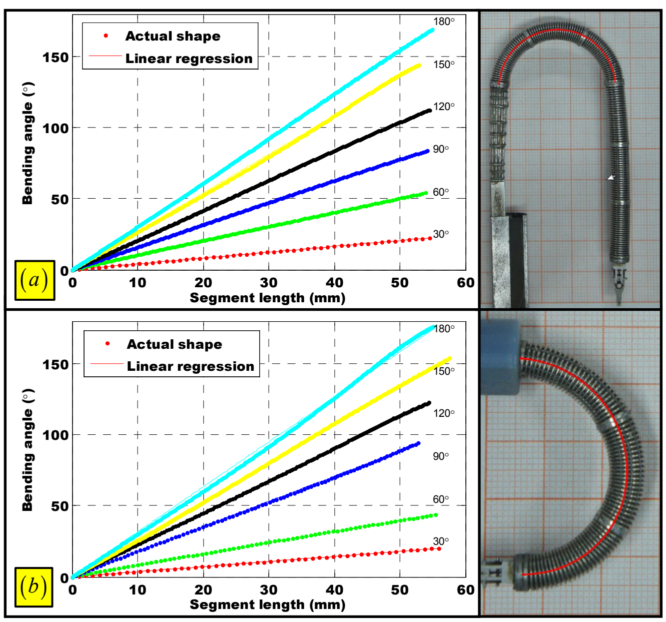

Fig. 8.Bending shape identification of (a) DS-1 and (b) DS-2

B. Distal Dexterity Enhancement

The kinematics in Section III.B quantifies the enhanced capabilities of the manipulation arms in terms of i) the enlarged translational workspace, and ii) the improved capabilities of orienting surgical end effectors.

The distal dexterity enhancement is expected to facilitate the surgical tasks, such as tissue peeling, knot tying, object placing, etc. However, it could be difficult to quantify how much improvements have been achieved for these tasks. In order to do so, dozens of surgeons shall be selected to operate the SURS till statistically meaningful data has been obtained to confirm these improvements.

Since the SURS might not be ready for massive trials, this paper hence proposes a more practical approach to measure the improved capability of orienting a surgical end effector.

The experimental setup is shown in Fig. 9(a). The gripper was commanded to move around the P_2 point, repeating the simulations in Fig. 7(a.2) and Fig. 7(b.2). A cover was used to hold a marker along the gripper's axis. Since the cover blocks the view to the gripper, a bead was placed at the P_2 point to ensure the rotation is indeed about the P_2 point. This experiment can also be viewed in the multimedia extension.

An optical tracker (Micron Tracker SX60, Claron Technology Inc.) was used to track the marker to give out orientations of the gripper. The orientations are transformed to the world coordinate $\{w\}$ and plotted in Fig. 9(d). $\{w\}$ is located at the base of the arm as shown in Fig. 5(b).

For the AL case, the orientations closely match the results as in Fig. 7(a.2). For the EB case, although the gripper can be more freely oriented than the AL case, the actual range is smaller than the simulated motion ranges as in Fig. 7(b.2).

A possible reason to explain this deviation is that bending of the DS-2 affects bending of the DS-1. When the DS-1 and the DS-2 are commanded, the actuation compensation from [14] was implemented. That compensation didn't consider the coupling in bending between the DS-1 and DS-2. When a larger bending is now allowed, the influences from the DS-2's bending to the DS-1's motions need to be properly handled in the actuation compensation.

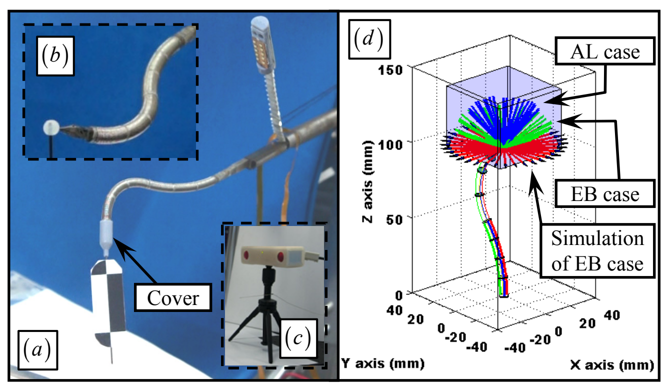

Fig. 9.Measurement of the distal dexterity: (a) the experimental setup, (b) rotation about a bead at the P_2 point, (c) the tracker, and (d) the results

C. Tissue Resection

The SURS's arm with a gripper could be replaced by an arm with a unipolar electrical cautery spatula. The arm with the cautery spatula has the same geometrical specifications and hence motion capabilities as the one with a gripper.

Tissue resecting tests were carried out on a piece of porcine liver with a gripper arm on the right and a cautery spatula arm on the left, as shown in Fig. 10: (a) the right arm lifted a piece of tissue up and (b) the left arm moved towards a desired position for resecting; (c) a pedal was used to initiate the cutting once the spatula was in contact with the tissue; (d) some smoke was generated during the resecting and (e) the resecting continued till the tissue was completely cut; (f) then the removed tissue could be extracted.

The tissue resection can also be viewed in the multimedia extension.

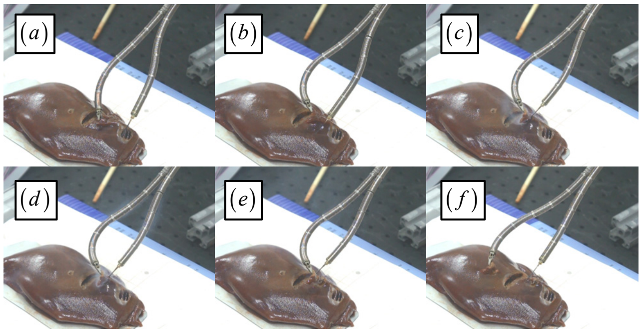

Fig. 10. Tissue resection experiments

V. Conclusions and Future Work

The SURS (SJTU Unfoldable Robotic System) for SPL was recently developed, aiming to achieve improved system specifications (e.g. a smaller incision port). It can be deployed into abdomen through a Ø12mm port in its folded form and can then be unfolded for dual-arm surgical manipulations.

During the ex-vivo experimentation, the SURS's motion capabilities were found to be worse than what were expected due to the limited extensions and contractions of its segments. In order to enhance the distal dexterity, this paper proposes to extend the kinematics model for bending beyond 90°, making full use of the arms' physically allowed bending ranges. With the circular-arc bending assumption verified up to a 180° bending, the simulation and experimental results quantified the improvements on the distal motion capabilities.

Moreover, a third arm with an electrical cautery spatula was fabricated and assembled into the SURS to realize tissue resection. Such a functionality enhancement pushed the SURS one more step towards future animal studies.

The coupling in bending between the adjacent segments might not be neglected any more, when the bending is beyond 90°. This coupling shall be properly handled in the actuation compensation which will be carried out soon. What's more, more exchangeable manipulation arms with different surgical end effectors (e.g., curved scissors, fenestrated forceps, clip applier, vessel sealer, suction tip, etc.) are to be fabricated to allow the SURS for more realistic tests in the future.

References

[1] G. Navarra, E. Pozza, S. Occhionorelli, P. Carcoforo, and I. Donini, "One-Wound Laparoscopic Cholecystectomy," *British Journal of Surgery,* vol. 84, No.5, p. 695, 1997.

[2] P. G. Curcillo II, A. S. Wu, E. R. Podolsky, C. Graybeal, N. Katkhouda, A. Saenz, R. Dunham, S. Fendley, M. Neff, C. Copper, M. Bessler, A. A. Gumbs, M. Norton, A. Iannelli, R. Mason, A. Moazzez, L. Cohen, A. Mouhlas, and A. Poor, "Single-Port-Access (SPA^{TM}) Cholecystectomy: a Multi-Institutional Report of the First 297 Cases," *Surgical Endoscopy,* vol. 24, No.8, pp. 1854-1860, 2010.

[3] Y. Sekiguchi, Y. Kobayashi, Y. Tomono, H. Watanabe, K. Toyoda, K. Konishi, M. Tomikawa, S. Ieiri, K. Tanoue, M. Hashizume, and M. G. Fujie, "Development of a Tool Manipulator Driven by a Flexible Shaft for Single Port Endoscopic Surgery," in *IEEE / RAS-EMBS International Conference on Biomedical Robotics and Biomechatronics (BIOROB)*, Tokyo, Japan, 2010, pp. 120-125.

[4] Y. Kobayashi, Y. Sekiguchi, T. Noguchi, Y. Takahashi, Q. Liu, S. Oguri, K. Toyoda, M. Uemura, S. Ieiri, M. Tomikawa, T. Ohdaira, M. Hashizume, and M. G. Fujie, "Development of a Robotic System with Six-Degrees-of-Freedom Robotic Tool Manipulators for Single-Port Surgery," *International Journal of Medical Robotics and Computer Assisted Surgery,* vol. Early View, 2014.

[5] H. Lee, Y. Choi, and B.-J. Yi, "Stackable 4-BAR Manipulators for Single Port Access Surgery," *IEEE/ASME Transaction on Mechatronics,* vol. 17, No.1, pp. 157-166, Feb 2012.

[6] B. Cheon, E. Gezgin, D. K. Ji, M. Tomikawa, M. Hashizume, H.-J. Kim, and J. Hong, "A Single Port Laparoscopic Surgery Robot with High Force Transmission and a Large Workspace," *Surgical Endoscopy,* vol. OnlineFirst, 2014.

[7] H. Samson, "Titan Medical Inc. Completes Functional Prototype of its Single Port Orifice Robotic Technology (SPORT(TM)) Surgical System," in *Marketwired* Toronto, Ontario, Canada, 2013.

[8] J. H. Kaouk, G.-P. Haber, R. Autorino, S. Crouzet, A. Ouzzane, V. Flamand, and A. Villers, "A Novel Robotic System for Single-port Urologic Surgery: First Clinical Investigation," *European Urology,* vol. In Press, 2014.

[9] M. Piccigallo, U. Scarfogliero, C. Quaglia, G. Petroni, P. Valdastri, A. Menciassi, and P. Dario, "Design of a Novel Bimanual Robotic System for Single-Port Laparoscopy," *IEEE/ASME Transactions on Mechatronics,* vol. 15, No.6, pp. 871-878, Dec 2010.

[10] G. Petroni, M. Niccolini, A. Menciassi, P. Dario, and A. Cuschieri, "A Novel Intracorporeal Assembling Robotic System for Single-Port Laparoscopic Surgery," *Surgical Endoscopy,* vol. 27, No.2, pp. 665-670, Feb 2013.

[11] K. Xu, R. E. Goldman, J. Ding, P. K. Allen, D. L. Fowler, and N. Simaan, "System Design of an Insertable Robotic Effector Platform for Single Port Access (SPA) Surgery," in *IEEE/RSJ International Conference on Intelligent Robots and Systems (IROS)*, St. Louis, MO, USA, 2009, pp. 5546-5552.

[12] J. Ding, R. E. Goldman, K. Xu, P. K. Allen, D. L. Fowler, and N. Simaan, "Design and Coordination Kinematics of an Insertable Robotic Effectors Platform for Single-Port Access Surgery," *IEEE/ASME Transactions on Mechatronics,* vol. 18, No.5, pp. 1612-1624, Oct 2013.

[13] K. Xu, M. Fu, and J. Zhao, "Design of the SJTU Unfoldable Robotic System (SURS) for Single Port Laparoscopy," in *IEEE International Conference on Robotics and Biomimetics (ROBIO)*, Bali, Indonesia, 2014, p. Accepted for presentation.

[14] K. Xu, J. Zhao, and M. Fu, "Development of the SJTU Unfoldable Robotic System (SURS) for Single Port Laparoscopy," *IEEE/ASME Transactions on Mechatronics,* vol. PP, No. 99, pp. 1-13, 2014.

[15] K. Xu and X. Zheng, "Configuration Comparison for Surgical Robotic Systems Using a Single Access Port and Continuum Mechanisms," in *IEEE International Conference on Robotics and Automation (ICRA)*, Saint Paul, MN, USA, 2012, pp. 3367-3374.

[16] K. Xu, J. Zhao, and X. Zheng, "Configuration Comparison among Kinematically Optimized Continuum Manipulators for Robotic Surgeries through a Single Access Port," *Robotica,* p. FirstView Article, 2014.

[17] K. Xu and N. Simaan, "An Investigation of the Intrinsic Force Sensing Capabilities of Continuum Robots," *IEEE Transactions on Robotics,* vol. 24, No.3, pp. 576-587, June 2008.

[18] K. Xu and N. Simaan, "Analytic Formulation for the Kinematics, Statics and Shape Restoration of Multibackbone Continuum Robots via Elliptic Integrals," *Journal of Mechanisms and Robotics,* vol. 2, No.011006, pp. 1-13, Feb 2010.

[19] R. J. Webster and B. A. Jones, "Design and Kinematic Modeling of Constant Curvature Continuum Robots: A Review " *International Journal of Robotics Research,* vol. 29, No.13, pp. 1661-1683, Nov 2010.

[20] K. Xu, M. Fu, and J. Zhao, "An Experimental Kinestatic Comparison between Continuum Manipulators with Structural Variations," in *IEEE International Conference on Robotics and Automation (ICRA)*, Hong Kong, China, 2014, p. Accepted for presentation.

[21] K. Xu and D. Qiu, "Experimental Design Verification of a Compliant Shoulder Exoskeleton," in *IEEE International Conference on Robotics and Automation (ICRA)*, Karlsruhe, Germany, 2013, pp. 3894-3901.